Static EUV microexposures using the ETS Set-2 optics

Patrick Naulleau[1], Kenneth A. Goldberg[1], Erik H. Anderson[1], Jeffrey Bokor[1,2], Bruce Harteneck[1], Keith Jackson[1], Deirdre Olynick[1], Farhad Salmassi[1], Sherry Baker[3], Paul Mirkarimi[3], Eberhard Spiller[3], Chris Walton[3], Donna O'Connell[4], Pei-Yang Yan[5], and Guojing Zhang[5]

[1]Center for X-Ray Optics, Lawrence Berkeley National Laboratory, Berkeley, CA 94720
[2]EECS Department, University of California, Berkeley, CA 94720
[3]Lawrence Livermore National Laboratory, PO Box 808, Livermore, CA 94550
[4]Sandia National Laboratories, PO Box 969, Livermore CA 94551
[5]Intel Corporation, 2200 Mission College Boulevard, Santa Clara CA 95052

ABSTRACT

While interferometry is routinely used for the characterization and alignment of lithographic optics, the ultimate measure of performance for these optical systems is the transfer of an image or pattern into photoresist. Simple yet flexible exposure systems play an important role in this task because they allow complex system-dependent effects to be isolated from the printing results. This enables the most direct lithographic evaluation of the optical system under investigation. To address these issues for commercial-class EUV optics, a synchrotron-based programmable illuminator exposure station has been implemented at Lawrence Berkeley National Laboratory (the Advanced Light Source). As previously presented, this static microfield exposure system has been used to lithographically characterize a 4-mirror optical system designed for the EUV Engineering Test Stand (ETS) prototype stepper.

Based on the lithographic characterization, here we present a detailed performance analysis of the 0.1-NA ETS Set-2 optic. Operation of the static printing system with the Set-2 optic yielded approximately 330 exposed wafers, where each wafer contains one or more focus-exposure matrices. A wide variety of parameters were studied including, among others, illumination conditions, resist thickness, and mask tone. Here we present a subset of this data in terms of process-window results. The results demonstrate a depth of focus (DOF) approximately 2 μm for isolated 70-nm line features, 1 μm for nested 70-nm line features, and 0.5 μm for 70-nm contacts on 270-nm pitch.

Keywords: extreme ultraviolet lithography, synchrotron radiation, microfield printing

1. INTRODUCTION

The lithographic resolution limits imposed by today's refractive optical systems has led to the development of various *next-generation lithography* techniques, of which extreme ultraviolet (EUV) projection lithography is now the leading contender. Because EUV systems utilize resonant reflective coatings,[1] at-wavelength characterization,[2-4] including system wavefront metrology, has played an essential role in the development of EUV lithographic optics. The ultimate measure of lithographic quality, however, is pattern transfer into photoresist as enabled by alpha class steppers such as the EUV Engineering Test Stand (ETS)[5] now operational at the Virtual National Laboratory (the VNL is a partnership between Lawrence Berkeley, Lawrence Livermore, and Sandia National Laboratories). Although ideal for the characterization of system-

Emerging Lithographic Technologies VII, Roxann L. Engelstad, Editor,
Proceedings of SPIE Vol. 5037 (2003) © 2003 SPIE · 0277-786X/03/$15.00

level issues, the complexity of the ETS limits its ability to systematically isolate the optical performance of the projection system from the rest of the system parameters such as illumination effects. To facilitate the lithographic characterization of the projection optic itself, a static microfield printing system has been implemented at Lawrence Berkeley National Laboratory's Advanced Light Source synchrotron radiation facility. These printing capabilities are integrated into the EUV phase-shifting point diffraction interferometer (PS/PDI)[3,4] experimental station, facilitating the direct comparison between wavefront metrology and printing results. In the printing configuration, the test station is referred to as the Static Exposure Station (SES).

A static imaging system, the SES has a microfield size of approximately 100 μm at the wafer. The SES works with the same reflection masks used in the ETS. In addition, the SES supports variable partial coherence (σ) ranging from approximately 0 to 1 and enables the generation of arbitrary pupil fills such as dipole and the ETS 6-channel fill. Moreover, because the pupil fill is synthesized through a scanning process,[6] as opposed to using apertures, modifying the pupil fill is achieved without loss of optical throughput.

As previously described,[7,8] the SES has been used to lithographically characterize the second of two EUV 4×-reduction optical systems[9] developed as part of the EUV LLC's lithography program. The first optic was a developmental set dedicated to fabrication and system integration learning, whereas the second much higher quality optic[10] is intended for EUV lithographic learning. Operation of the SES with the Set-2 optic yielded approximately 330 wafers, where each wafer is comprised of at least one focus-exposure matrix (FEM). A wide variety of parameters were studied including, illumination, resist, and mask tone. Here we present a subset of this data in terms of the process window. We note that since completion of the static microfield characterization described here, the Set-2 optic has been integrated into the ETS.[11]

2. SYSTEM CONFIGURATION

As described above, the SES is a static system allowing simple stages to be used. For optimal compatibility between interferometry and printing modes, the same stages are used in the two configurations. One drawback of this is that the total stage travel is limited to approximately 2 mm, limiting the potential size of the FEM. However, due to the small 100-μm field size, as constrained by the illuminator design, FEMs with up to approximately 20 elements in one direction can be printed.

Although the instantaneous static field size is limited to 100 μm, the full 1-inch arc-shaped field of view can be covered one subfield at a time by moving the entire system (with the exception of the illuminator components) under the beam. The reticle stage, optic, and wafer stage are all integrated into a single rigid structure that can be moved as a unit using a precise planar-bearing structure. This same mechanism is used during the interferometry to probe the wavefront at various field points.

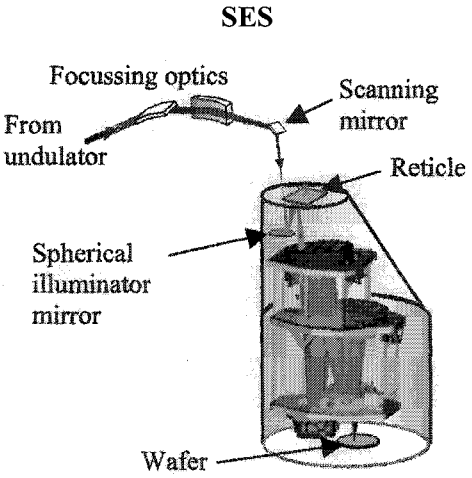

Fig. 1. Schematic of the SES. A scanning mirror serves as the decoherentizing element allowing the intrinsically coherent undulator source to be used for lithographic printing.

To enhance relevance of the printing results, the SES has been designed to operate with conventional reflection masks. We note, however, that illumination constraints (Fig. 1) force the imaged area to be within a few mm of the edge of the mask. To prevent problems associated with multilayer deposition and patterning variations near the edge of the mask, the pattern is actually located near the center of a 6-inch mask and the mask is cut into two 3×6-inch segments after completion of the mask fabrication process.

A crucial component of the SES is the coherence-controlling illuminator. Because the undulator is optimized for the high spatial coherence demanded by high-accuracy wavefront metrology,[12,13] steps must be taken to make the illumination appropriate for lithography. This issue has been addressed by implementing an active illumination system where the final illuminator element is a spherical mirror designed to re-image a scanning mirror to the reticle. The scanning mirror can be viewed as the effective source of a *critical* illumination system. By scanning the mirror comprising the effective source in angle, the source spatial-frequency content can be arbitrarily defined. Noting that the spatial coherence properties of a source are simply related to the Fourier transform of the source spatial spectrum (Van Cittert-Zernike Theorem),[14] it is evident that the illumination coherence properties can be controlled through the definition of the source scanning.

It is important to note that the coherence control described above assumes the observation time to be long relative to the scan rate. In practice this means that the lithographic exposure time should be at least as long as it takes to fully scan the desired pupil fill once. Additionally, the exposure time should be an integer multiple of the full pupil fill scan time. In the case of a typical $\sigma = 0.7$ pupil fill, the full pupil scan time is approximately 1 second, set by the mechanical resonance of the 2-D scanner. In practice we cycle through the pupil fill at least four times for improved uniformity; thus, a typical SES exposure is four seconds long. We note that were the scan time not a limiting factor, the undulator beamline would have enough power to support millisecond exposures in the 100-μm SES microfield.

3. PRINTING CHARACTERIZATION

We begin by considering the resolution limit of the characterized Set-2 optic at best focus. Figure 2 shows a series of equal line-space images ranging from a half-pitch of 100 nm down to 60 nm. The features were printed using a darkfield mask where each 9-bar pattern is positioned in a local brightfield slightly larger than the 9-bar pattern itself. Figure 3 shows a scanning electron microscope (SEM) image of the 100-nm coded features on the mask. The resist images shown in Fig. 2 were all recorded in Shipley EUV 2D resist under conventional disk illumination with a σ of 0.8. Because the ETS Set-2 optic[9] has a numerical aperture (NA) of 0.1, these prints correspond to k_1 factors of 0.75 through 0.45, where k_1 is defined as $(CD)(NA)/\lambda$. We note that utilizing dipole illumination the Set-2 optic has previously been demonstrated[7] to be capable of 50-nm half pitch printing ($k_1 = 0.375$). Extrapolating these results to an EUV optic with 0.25 NA (the expected NA of the first EUV Beta tools), 40-nm CD would correspond to a k_1 factor of 0.75, equivalent to the 100-nm CD prints presented here. Moreover, achieving a k_1 factor of 0.45 (as achieved here with conventional illumination) with an NA of 0.25 would result in 24-nm half-pitch printing.

Through exposure control, it is possible to further reduce k_1 for loose-pitch features. Figure 4 shows 37-nm lines on 240-nm pitch as well as an isolated 41-nm line. As coded on the mask, these features were 80-nm and 70-nm, respectively. These results were obtained using conventional disk illumination with a σ of 0.7.

Although Fig. 2 demonstrates resolution down to 60-nm half pitch, a practical measure of the achievable resolution must be based on process-window size, or depth of focus (DOF) at a given exposure latitude (EL). The process-window results presented here correspond to +/-10% CD change and the DOF is quoted with 10% EL. Figures 5 through 8 show Bossung plots and corresponding process window plots for half-pitches down to 70 nm. The 60-nm case is not shown as no measurable process window was found. The plot in Fig. 9 shows a summary of the DOF results through half pitch. At 100-nm CD, a DOF of approximately 2 μm is observed with the DOF dropping approximately linearly to 0.8 μm at a CD of 70 nm.

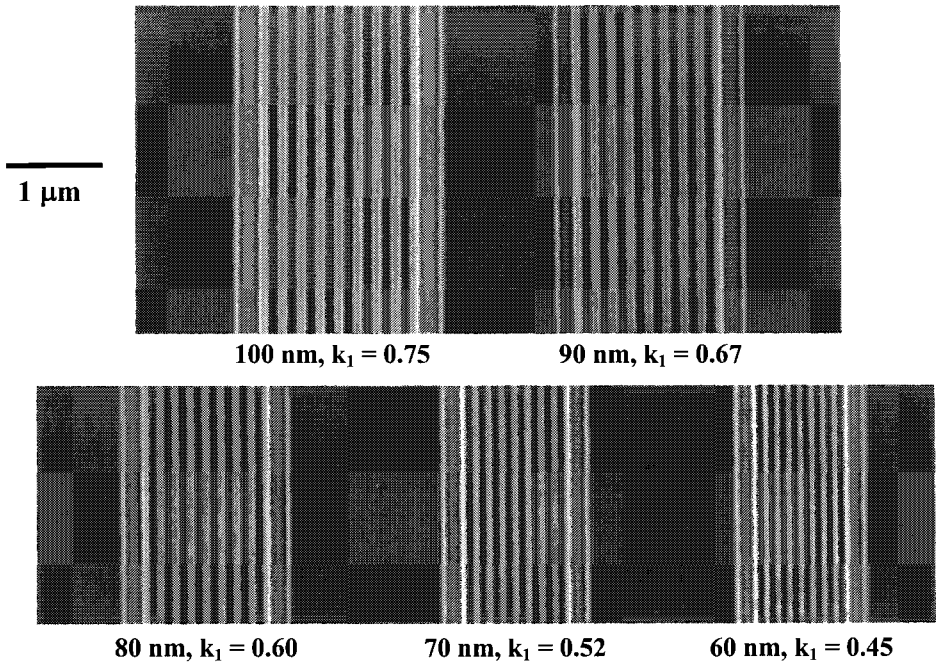

Fig. 2. Series of dense-line images ranging from 100-nm CD down to 60-nm CD. All images were recorded with conventional disk illumination and a partial coherence of 0.8.

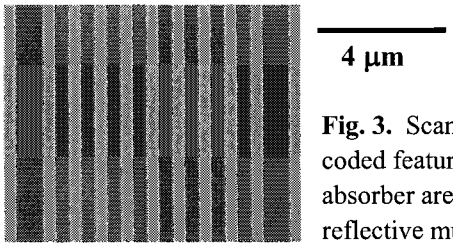

Fig. 3. Scanning electron microscope image of the 100-nm coded features on the mask. Light areas correspond to absorber areas (lines) and dark areas correspond to reflective multilayer areas (clear areas or spaces).

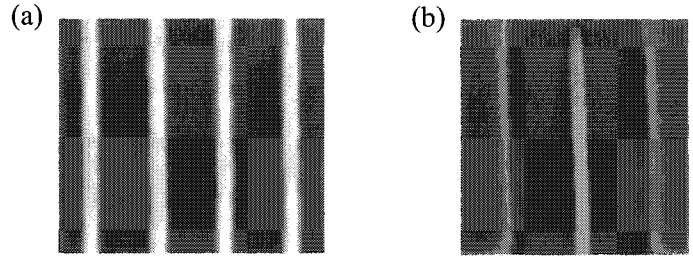

Fig. 4. (a) 37-nm lines on 240-nm pitch and (b) 41-nm isolated line.

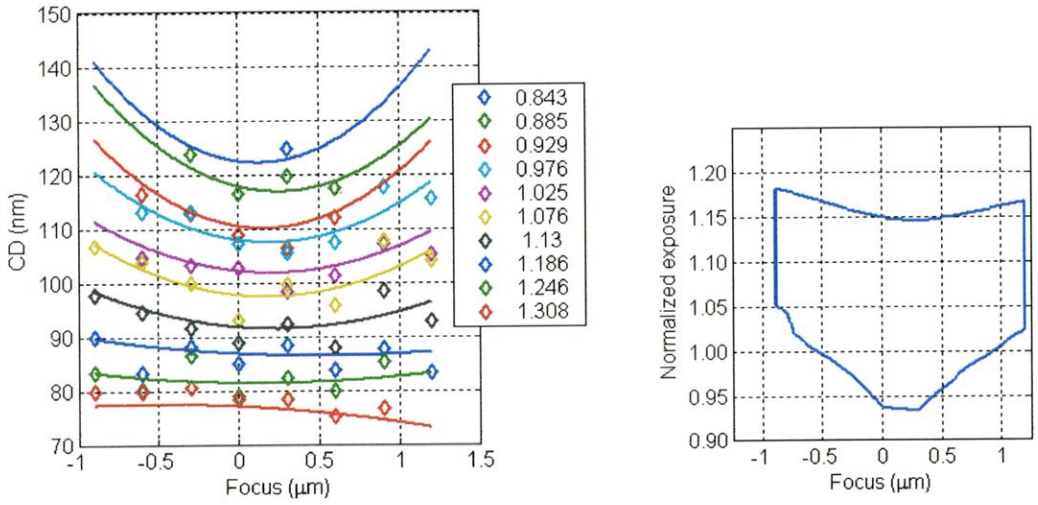

Fig. 5. +/-10% CD change process-window results for 100-nm half-pitch features. The legend values represent the normalized dose.

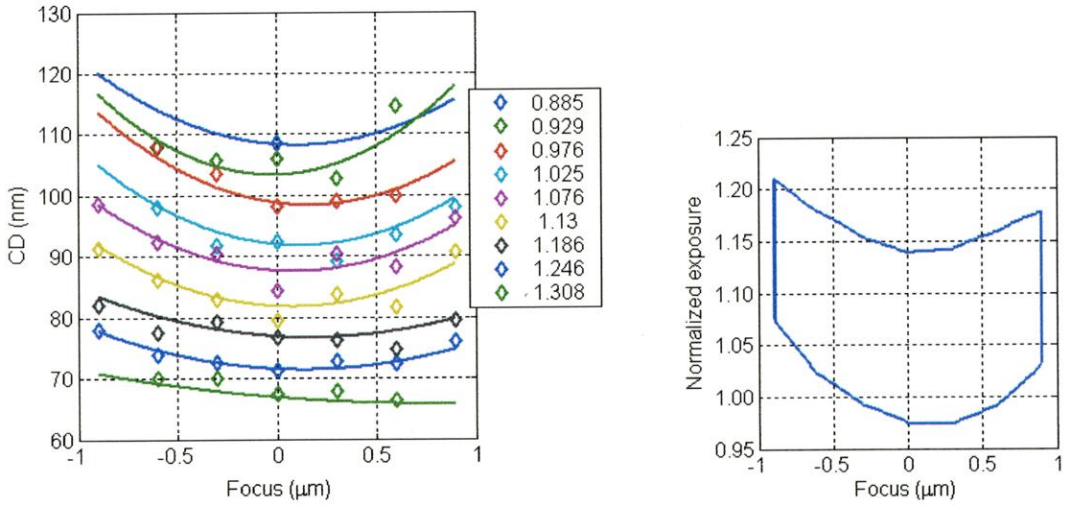

Fig. 6. +/-10% CD change process-window results for 90-nm half-pitch features.

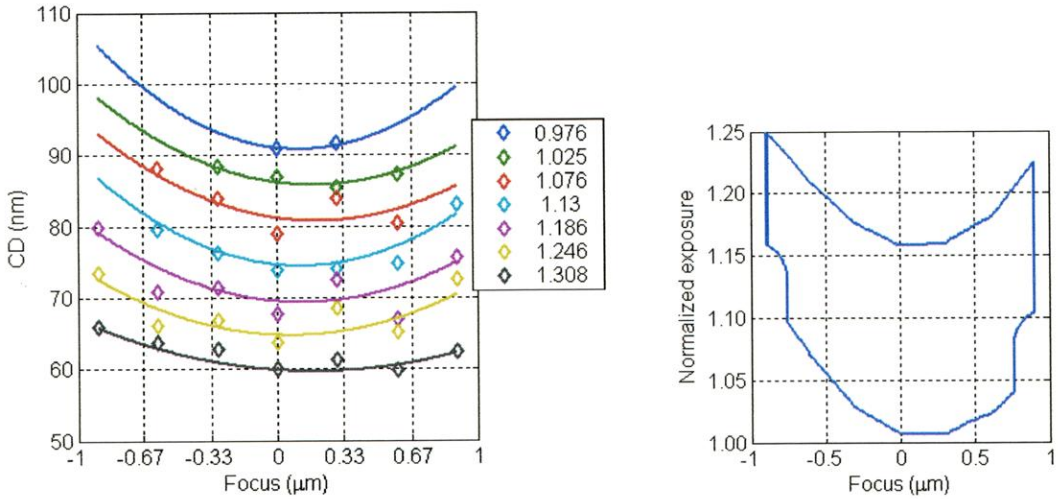

Fig. 7. +/-10% CD change process-window results for 80-nm half-pitch features.

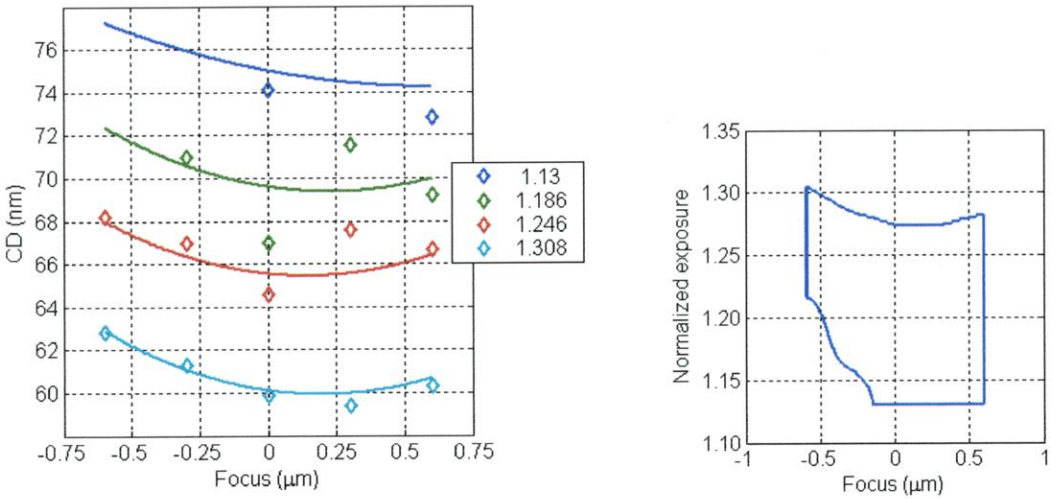

Fig. 8. +/-10% CD change process-window results for 70-nm half-pitch features.

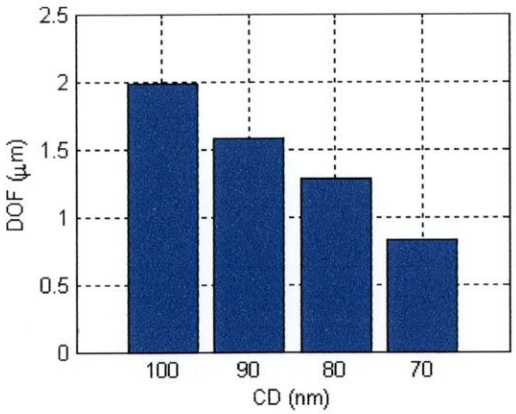

Fig. 9. DOF as a function of CD based on the process window results from Figs. 3 through 6 and an EL of 10%

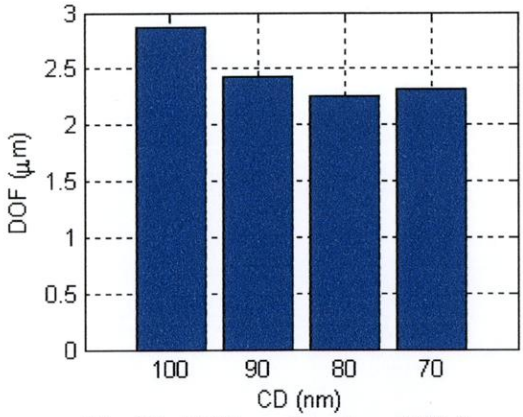

Fig. 10. DOF as a function of CD for isolated line features using the same criteria as used in Fig. 7

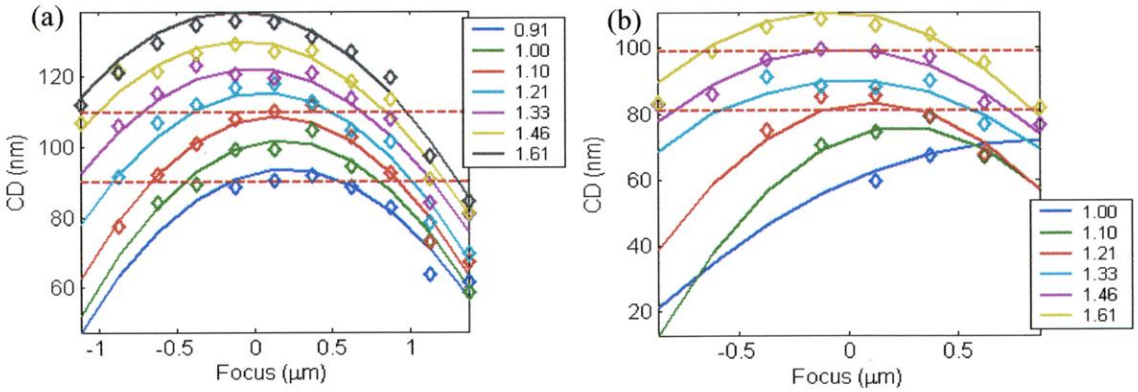

Fig. 11. Bossung plots for contacts coded as (a) 100/300 nm CD/pitch and (b) 90/270 nm CD/pitch.

Repeating the same analysis on FEM data from isolated features yields the DOF results in Fig. 10. For the isolated line features we see an increased DOF relative to the nested features and we also notice a decreased sensitivity of DOF to CD. Better than 2 μm DOF is demonstrated down to 70-nm CD. The Bossung plots show both the measured data (symbols) and fitted data (lines) used in the actual determination of the process window. The fitted data is based on two-dimensional fitting of the CD surface through both dose and focus, explaining the apparent discrepancies seen between some of the fits and the plotted one-dimensional through-focus data. This method minimizes the impact of our experimental dose uncertainty, which is on the order of 2%.

Finally we consider the process window on loose-pitch contacts. Figure 11 shows the Bossung plots for contacts coded as 100/300 nm CD/pitch and 90/270 nm CD/pitch, respectively. Extracting the DOF yields 1.3 mm for 100-nm CD and 1.0 for 90-nm CD. We note that analyzing the 90-nm coded results in the underdosed condition allows us to extract DOF results at CDs of 80 nm and 70 nm. However, because these 80-nm and 70-nm results are derived from 90-nm coded features, the pitch remains 270-nm. Figure 12 summarizes the DOF results on the loose-pitch contacts.

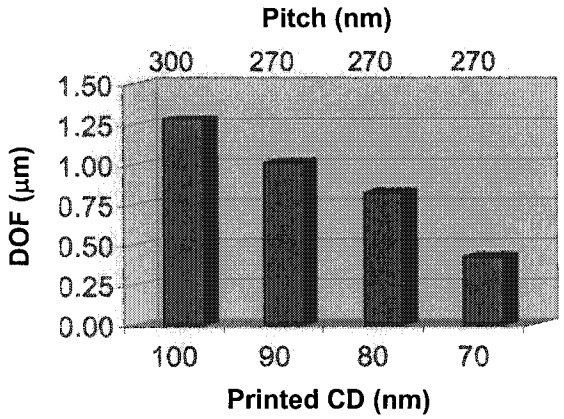

Fig. 12. Summary of DOF results on loose-pitch contacts. The 100-nm contacts have 300-nm pitch and the 90-nm through 70-nm contacts have 270-nm pitch.

4. SUBSTRATE DEFECT PRINTABILITY TESTS

In addition to lithographical characterization the ETS Set-2 optic, the SES has verified the effectiveness of recently developed defect-smoothing techniques.[15] In these techniques, the multilayer deposition process itself is used to reduce the printability of defects (or particles) present on the substrate. The availability of such a technique can, in principle, greatly reduce the cost of EUV masks and in turn the cost of ownership of EUV lithography.[16] One particularly promising technique uses ion-beam deposition with additional ion-assisted polishing employed at each layer.[17,18]

To enable quantitative lithographic testing of proximity effects, a programmed substrate defect mask fabrication process was developed.[15] The relevant defect sizes on the substrate are on the order of 50×50×50 nm. Defect patterning was performed using electron-beam lithography to directly pattern a spin-on-glass resist (HSQ).[19] The resist relief features remaining after processing, which take the form of highly-robust silicon dioxide, serve as the programmed defects. This same technology has recently been used to fabricate high-efficiency reflective blazed-phase gratings operating at EUV wavelengths.[20]

For comparison purposes, two identical programmed substrates were fabricated, one coated with a conventional ion-beam deposited multilayer and the second using the smoothing-enhanced process. After coating, both masks were patterned with an absorber line-space pattern in controlled proximity to the defects using the same electron-beam lithography tool[21] employed to fabricate the defects.

Figure 13 shows an AFM image from one of the masks immediately following the defect layer fabrication. The image is of a set of four 50-nm-wide, 50-nm tall defects. The large 2-um-wide feature, also patterned in HSQ, was added as a locating feature for pre- and post-coating metrology.

Figure 14 shows in-focus nominal dose images of defects in proximity to 100-nm lines as coded. The defects are nominally centered in the line-space pattern. The labels associated with each

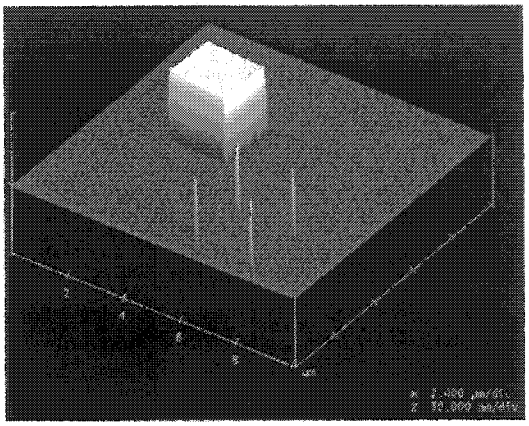

Fig. 13. AFM image from one of the masks immediately following the defect layer fabrication. The image is of a set of four 50-nm-wide, 50-nm tall defects. The large 2-um-wide feature, also patterned in HSQ, was added as a locating feature. Z-scale is exaggerated for visualization.

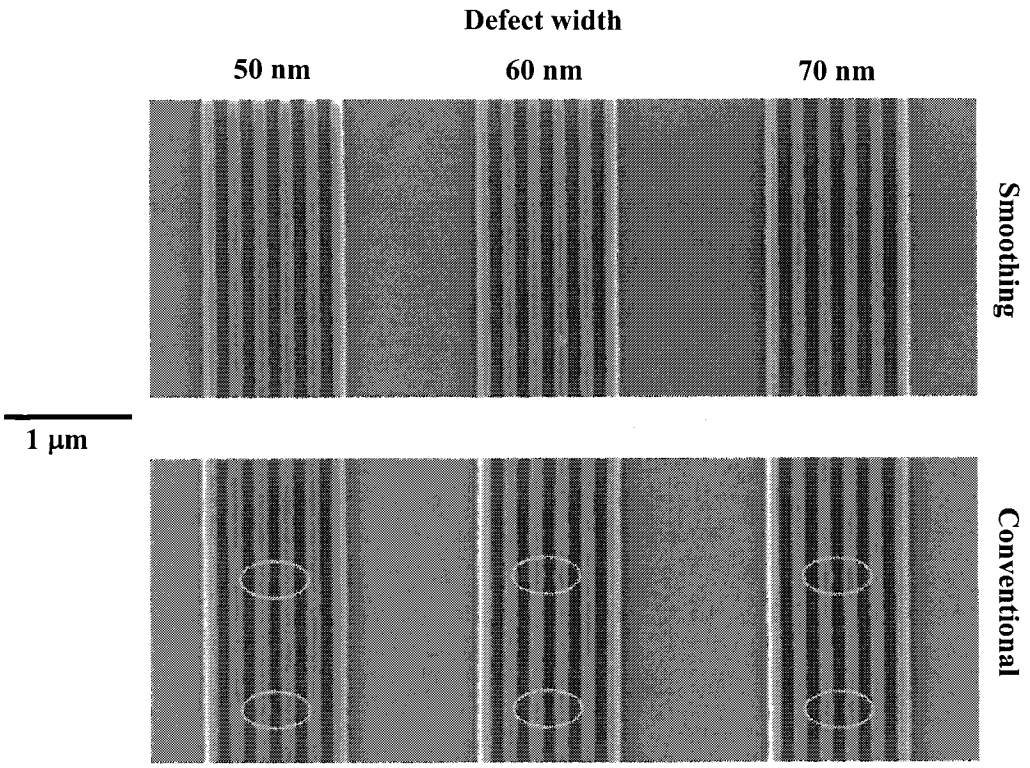

Fig. 14. Defect-printability exposure studies results. SEM images printed 100-nm lines and spaces with embedded proximity defects of widths ranging from 50 nm to 70 nm. Results using both smoothing-optimized (a) and conventional ion-beam deposited (b) multilayers are shown. These images were recorded at best focus and close to nominal dose. Where visible, the defect effects on the proximity line widths are circled.

column correspond to the lateral defect dimension with all defects being 50-nm tall. The top row shows the smoothing enhanced case and the bottom row the conventional multilayer case. It is evident that smoothing renders 70-nm defects unprintable at best focus, whereas without smoothing, even 50-nm defects are printable at focus. Where visible, the defect effects on the proximity line widths are circled. We note that full process-window analysis[15] has shown that the actual printablility cutoff given the present smoothing technology is approximately 60-nm. This is more restrictive than one might predict simply from Fig. 14 because the printability increases with defocus.

5. SUMMARY

The static microfield exposure station installed at Lawrence Berkeley National Laboratory's Advanced Light Source synchrotron radiation facility has been used to lithographically characterize the Set-2 optic, which is now integrated into the ETS. These results serve both as a source for valuable EUV learning and as a performance benchmark for operation of the ETS with the Set-2 optic. Process-window results on equal line/space features show approximately a 2-μm DOF when operating at a k_1 factor of 0.75 (100-nm CD) and nearly 1-μm DOF at 70-nm CD. On isolated features, better than 2-μm DOF is achieved all the way down to 70-nm CD. Also, printing of 70-nm contacts on 270-nm pitch has been demonstrated to support a DOF of nearly 0.5 μm. Finally, mask-defect-printability studies have demonstrated that 60-nm substrate defects are rendered unprintable throughout the process window using appropriate multilayer smoothing techniques.

6. ACKNOWLEDGEMENTS

The authors are greatly indebted to Kevin Bradley, Rene Delano, Paul Denham, Brian Hoef, Gideon Jones, Seno Rekawa, Ron Tackaberry, and Eugene Veklerov for expert engineering and fabrication support, and to the entire CXRO staff for enabling this research. This research was supported by the Extreme Ultraviolet Limited Liability Company and the DOE Office of Basic Energy Science.

REFERENCES

1. J. H. Underwood and T. W. Barbee, Jr., "Layered synthetic microstructures as Bragg diffractors for X rays and extreme ultraviolet: theory and predicted performance," Appl. Opt. **20**, 3027-3034 (1981).
2. D. Attwood, G. Sommargren, R. Beguiristain, K. Nguyen, J. Bokor, N. Ceglio, K. Jackson, M. Koike, and J. Underwood, "Undulator radiation for at-wavelength interferometry of optics for extreme-ultraviolet lithography," Appl. Opt. **32**, 7022-7031 (1993).
3. H. Medecki, E. Tejnil, K. A. Goldberg, and J. Bokor, "Phase-shifting point diffraction interferometer," Opt. Lett. **21**, 1526-1528 (1996).
4. K. A. Goldberg, P. Naulleau, P. Batson, P. Denham, H. Chapman, and J. Bokor, "Extreme ultraviolet alignment and testing of a four mirror aspheric extreme ultraviolet optical system," J. Vac. Sci. and Technol. B **18**, 2911-15 (2000).
5. D. A. Tichenor, G. D. Kubiak, M. E. Malinowski, R. H. Stulen, S. J. Haney, K. W. Berger, R. P. Nissen, R. L. Schmitt, G. A. Wilkerson, L. A. Brown, P. A. Spence, P. S. Jin, W. C. Sweat, W. W. Chow, J. E. Bjorkholm, R. R. Freeman, M. D. Himel, A. A. MacDowell, D. M. Tennant, O. R. Wood II, W. K. Waskiewicz, D. L. White, D. L. Windt, and T. E. Jewell, "Development and characterization of a 10× Schwarzschild system for SXPL," in *OSA Proceedings on Soft X-Ray Projection Lithography,* Vol. **18**, A. M. Hawryluk and R. H. Stulen, eds., (Optical Society of America, Washington, DC, 1993), pp. 79-82.

6. P. Naulleau, K. Goldberg, P. Batson, J. Bokor, P. Denham, and S. Rekawa, "A Fourier-synthesis custom-coherence illuminator for EUV microfield lithography," Appl. Opt., *to be published* (2003).
7. P. Naulleau, K. Goldberg, E. Anderson, D. Attwood, P. Batson, J. Bokor, P. Denham, E. Gullikson, B. Hoef, K. Jackson, S. Rekawa, F. Salmassi, K. Blaedel, H. Chapman, L. Hale, R. Soufli, E. Spiller, D. Sweeney, J. Taylor, C. Walton, G. Cardinale, A. Ray-Chaudhuri, A. Fisher, G. Kubiak, D. O'Connell, R. Stulen, D. Tichenor, C. Gwyn, P. Yan, G. Zhang, "Static microfield printing at the Advanced Light Source with the ETS Set-2 optic," Proc. SPIE Vol. **4688**, 64-71 (2002).
8. P. Naulleau, K. Goldberg, E. Anderson, D. Attwood, P. Batson, J. Bokor, P. Denham, E. Gullikson, B. Harteneck, B. Hoef, K. Jackson, D. Olynick, S. Rekawa, F. Salmassi, K. Blaedel, H. Chapman, L. Hale, P. Mirkarimi, R. Soufli, E. Spiller, D. Sweeney, J. Taylor, C. Walton, D. O'Connell, R. Stulen, D. Tichenor, C. Gwyn, P. Yan and G. Zhang, "Sub-70-nm EUV Lithography at the Advanced Light Source Static Microfield Exposure Station Using the ETS Set-2 Optic," J. Vac. Sci. & Technol. B **20**, 2829-2833 (2002).
9. D. W. Sweeney, R. Hudyma, H. N. Chapman, and D. Shafer, "EUV optical design for a 100 nm CD imaging system," in *Emerging Lithographic Technologies II*, Y. Vladimirsky, ed., Proc. SPIE **3331**, 2-10 (1998).
10. K. Goldberg, P. Naulleau, J. Bokor, and H. Chapman, "Honing the accuracy of extreme ultraviolet optical system testing: at-wavelength and visible-light measurements of the ETS Set-2 projection optic," Proc. SPIE Vol. **4688**, 329-337 (2002).
11. D. O'Connell, S. Lee, D. Tichenor, W. Ballard, L. Bernardez, P. Barr, J. Goldsmith, Steve J. Haney, K. Jefferson, T. Johnson, A. Leung, W. Replogle, P. Naulleau, H. Chapman "Full-Field Lithographic Evaluation of POB2 in the Engineering Test Stand," *these proceedings.*
12. D. Attwood, P. Naulleau, K. Goldberg, E. Tejnil, C. Chang, R. Beguiristain, P. Batson, J. Bokor, E. Gullikson, H. Medecki, and J. Underwood, "Tunable coherent radiation in the soft X-ray and extreme ultraviolet spectral regions," IEEE J. Quantum Electron. **35**, 709-720 (1999).
13. C. Chang, P. Naulleau, E. Anderson, and D. Attwood, "Spatial coherence characterization of undulator radiation," Opt. Comm. **182**, 25-34 (2000).
14. J. W. Goodman, *Statistical Optics*, John Wiley & Sons, New York, 1986, **Chap. 5**, 157-229.
15. P. Naulleau, K. Goldberg, E. Anderson, J. Bokor, E. Gullikson, B. Harteneck, K. Jackson, D. Olynick, F. Salmassi, S. Baker, P. Mirkarimi, E. Spiller, C. Walton, and G. Zhang "Lithographic characterization of the printability of programmed EUV substrate defects," *submitted to J. Vac. Sci. & Technol. B* (2003).
16. P. Mirkarimi, E. Spiller, D. Stearns, V. Sperry, S. Baker, "An ion-assisted Mo-Si deposition process for planarizing reticle substrates for extreme ultraviolet lithography," IEEE J. Quantum Electron. **37**, 1514-1516 (2001).
17. P. Mirkarimi, E. Spiller, D. Stearns, S. Baker, V. Sperry, and E. Gullikson, "Developing a viable multilayer coating process for extreme ultraviolet lithography reticles," *in preparation.*
18. S. Hector, "EUVL masks: requirements and potential solutions," Proc. SPIE Vol. **4688**, 134-149 (2002).
19. F. van Delft, J. Weterings, A. van Langen-Suurling, H. Romijn, "Hydrogen silsesquioxane/novolak bilayer resist for high aspect ratio nanoscale electron-beam lithography," J. Vac. Sci. Technol. B **18**, 3419-3423 (2000).

20. P. Naulleau, E. Anderson, E. Gullikson, and J. Bokor, "Fabrication of high-efficiency multilayer-coated binary blazed gratings in the EUV regime," Opt. Comm. **200**, 27-34 (2001).

21. E. H. Anderson, D. L. Olynick, B. Harteneck, E. Veklerov, Gregory Denbeaux, W. Chao, A. Lucero, L. Johnson, and D. Attwood, "Nanofabrication and diffractive optics for high-resolution x-ray applications," J.Vac. Sci. Technol. B **18**, 2970-2975 (2000).